RSC Advances

PAPER



Cite this: *RSC Adv.*, 2023, **13**, 15401

# Preparation and characterization of diphenyl silicone rubber/microfiber glass wool composite thermal control films

Lin Li,[a] Xin Fu,[b] Xiang Xu, *[a] Dafu Wei[a] and Yong Guan *[a]

Innovative research on the development of thermal control films for spacecraft surfaces is presented. A hydroxy-terminated random copolymer of dimethylsiloxane–diphenylsiloxane (PPDMS) was prepared from hydroxy silicone oil and diphenylsilylene glycol by a condensation reaction, and then liquid diphenyl silicone rubber base material (denoted as PSR) was obtained by adding hydrophobic silica. Microfiber glass wool (MGW) with a fiber diameter of ~3 μm was added to the liquid PSR base material, which upon solidifying at room temperature, formed a 100 μm thick PSR/MGW composite film. The infrared radiation properties, solar absorption, thermal conductivity, and thermal dimensional stability of the film were evaluated. Moreover, the dispersion of the MGW in the rubber matrix was confirmed by optical microscopy and field-emission scanning electron microscopy. The PSR/MGW films exhibited a glass transition temperature of −106 °C, thermal decomposition temperature exceeding 410 °C, and low $\alpha/\varepsilon$ values. The homogeneous distribution of MGW in the PSR thin film resulted in a notable reduction in its linear expansion coefficient, as well as its thermal diffusion coefficient. Consequently, it exhibited a significant capacity for thermal insulation and retention. For the sample with 5 wt% of MGW, the linear expansion coefficient and thermal diffusion coefficient at 200 °C were reduced to 0.53% and 2.703 mm $s^{-2}$, respectively. Thus, the PSR/MGW composite film has good heat-resistance stability and low-temperature endurance, along with low $\alpha/\varepsilon$ values and excellent dimensional stability. Additionally, it facilitates effective thermal insulation and temperature control, and can be an ideal material for thermal control coatings on spacecraft surfaces.

Received 31st March 2023
Accepted 15th May 2023

DOI: 10.1039/d3ra02118a

rsc.li/rsc-advances

## Introduction

Thermal control coatings are a specific type of coating applied to spacecraft surfaces to achieve thermal control by adjusting the thermal and optical properties of the surface. They are one of the essential temperature control measures to ensure the proper operation of spacecraft equipment and to extend their service life.[1,2] The thermal control principle of these coatings involves regulating the spacecraft's surface reflection of UV-visible light and its absorption and emission of infrared radiation, resulting in thermal exchange between the interior and exterior environments. This is achieved through the differential solar absorptance ($\alpha$) and infrared emittance ($\varepsilon$) of various materials to control the temperature fluctuations of internal equipment, thereby ensuring their proper functionality when a spacecraft is at the alternating temperature range of −100–300 °C.[3–7]

One of the most extensively applied second surface mirror (SSM) thermal control coatings comprises a vacuum-deposited metal base layer and a surface thin film. The visible-light reflectivity of the vacuum-deposited metal base layer determines the solar absorptance, $\alpha$ of the second surface mirror, and the surface thin-film layer strongly absorbs infrared radiation while being transparent to visible light. Therefore, the infrared emittance, $\varepsilon$ of the second surface mirror depends on the thickness of the surface thin film.[8–10]

The currently used SSM coatings are mainly polyimide/Al and fluoropolymer/Ag. Both polyimide and fluoropolymer are high temperature resistant resins with high infrared emittance $\varepsilon$ and good light transmittance. However, they are not easy to be processed and modified due to their high melt point. Moreover, their low temperature resistance and atomic oxygen resistance are still insufficient.[11] Organosilicon coatings are much easier to be processed and modified, and have strong resistance to atomic oxygen erosion and vacuum UV radiation. In addition, surface coatings formed by cured organosilicon materials have good adhesion and cleaning properties, which render them ideal organic thermal control coatings for spacecraft and satellite surfaces.[12,13] In the study of atomic-oxygen effects, organosilicon materials were found to generate an inert

[a]*School of Materials Science and Engineering, Shanghai Key Laboratory of Advanced Polymeric Materials, East China University of Science and Technology, Shanghai, 200237, China. E-mail: xiangxu@ecust.edu.cn; yguan@ecust.edu.cn*
[b]*Shanghai Institute of Satellite Engineering, Shanghai, 201109, China*

inorganic silica layer *via* the oxidation of the Si–C bonds under the action of atomic oxygen, and the so-formed silica layer protected the underlying material from further corrosion by atomic oxygen. On the other hand, glass fibers do not react with atomic oxygen.[14–17] In studies on UV radiation resistance, polydimethylsiloxane (PDMS) without phenyl groups was found to undergo both radiation-induced crosslinking and degradation under UV light radiation, whereas PDMS with phenyl groups did not exhibit significant changes in its crosslinking density or dynamic mechanical properties.[18–20] In fact, the UV radiation resistance of phenyl group-containing PDMS was found to increase with an increase in the phenyl group content.[21] Li *et al.* reported that organosilicon materials prepared by physical blending have a more uniform structure and better optical transmittance than those prepared by solution copolymerization.[22]

In this study, a composite thermal control film composed of diphenyl silicone rubber and microfiber glass wool (MGW) cured at room temperature was used as the surface layer of the second surface mirror thermal control coating. Phenyl groups were introduced into the silicone rubber to improve its heat-resistance stability and UV radiation resistance, inhibit its crystallization at low temperatures, and enhance its overall stability. The effects of the MGW content on the mechanical, optical, and thermal properties of the composite coatings were studied. The composite thermal control films had low $\alpha/\varepsilon$ values, meeting the requirements of the surface thin-film material that can be applied as the second surface mirror-type thermal control coating. The composite coating has potential to be applied in the aerospace field.

# Experimental

## Materials

Hydroxy-terminated silicone oil (industrial grade) was purchased from Beijing InnoChem Science & Technology Co., Ltd, Beijing, China. Diphenylsilanediol (99.5%), NaOH, and glacial acetic acid (analytical reagent) were obtained from Sinopharm Chemical Reagent Co., Ltd. Hydrophobic nanosilica was prepared in the laboratory. MGW (BR) was procured from Shanghai Titan Scientific Co., Ltd, Shanghai, China. Silicon dioxide, aluminum oxide (99.5%), tetraethyl orthosilicate (analytical reagent), and dibutyltin dilaurate (95%), were purchased from Shanghai Macklin Biochemical Technology Co., Ltd, Shanghai, China.

## Synthesis of hydroxy-terminated random copolymer of dimethylsiloxane–diphenylsiloxane (PPDMS)

To synthesize PPDMS, 45.0 g of hydroxy-terminated polydimethylsiloxane and 5.0 g of diphenylsilanediol were added to a 100 mL three-necked flask. The resulting mixture was stirred at 140 °C for 30 min until the diphenylsilanediol was completely dissolved. The oil bath temperature was then lowered to 110 °C, and 0.05 g of NaOH was added to the mixture to initiate the reaction. Subsequently, nitrogen gas was slowly bubbled through the reaction mixture to remove the water produced during the reaction. After 30 min of reaction, the mixture was cooled to below 50 °C, and 0.075 g of ice-cold acetic acid was added to neutralize it. The resulting mixture was filtered to remove NaCl and any unreacted diphenylsilanediol, and PPDMS was collected. The viscosity of the product was 4423 mP s, while its molecular weight and molecular weight distribution were determined to be 5600 g $mol^{-1}$ and 2.99, respectively. The synthetic scheme of PPDMS is shown in Fig. 1.[23–25]

## Preparation of thin films of diphenylsiloxane rubber (PSR)

According to the formulation shown in Table 1, PPDMS, hydrophobic nanoscale $SiO_2$, and functional fillers (MGW, 5 μm silica, or 5 μm alumina) were added to a mortar in sequence. The resulting mixture was ground for 20 min until the filler particles were uniformly dispersed in the rubber matrix.

Subsequently, 0.5 g of tetraethyl orthosilicate and 0.1 g of dibutyltin dilaurate were added to the rubber and blended by grinding at room temperature for 10–15 min until a uniform, paste-like material was formed. The resulting diphenylsiloxane rubber/filler composite (hereafter referred to as the PSR/filler composite; see Table 1 for sample codes) was then scraped onto a smooth, clean polyethylene terephthalate (PET) film surface using a 100 μm film applicator to form a thin film. The film was aged at room temperature for 24 h and then peeled off and washed with deionized water under ultrasonication for 30 min. The composite film was then cured for 4 h in an aging oven at 200 °C to remove any remaining crosslinking agents and small molecules, resulting in the complete solidification of PSR/filler composite film. Fig. 2 shows the scheme of the preparation of the PSR/MGW composite films. This process yielded a series of PSR/filler composite films with different inorganic fillers. The diphenylsiloxane rubber film formed without the filler (denoted as PSR) was used as the control group.

## Structural characterization and performance evaluation

**$^{1}$H and $^{29}$Si NMR spectroscopic analyses.** A 400 MHz superconducting Fourier transform NMR spectrometer (Advance III 400, Bruker, Switzerland) was used to record the spectra of the samples dissolved in deuterated acetone as the solvent. Tetramethylsilane was used as the internal standard for $^{1}$H NMR spectroscopy, and acetylacetone chromium was employed as the relaxation agent for $^{29}$Si NMR spectroscopy.

**Gel permeation chromatography (GPC).** GPC was conducted using a single detection gel permeation chromatograph (Waters 1515, Waters, USA) using tetrahydrofuran as the mobile phase and polystyrene as the standard. The flow rate was set to 1 mL $min^{-1}$, and the testing temperature was maintained at 35 °

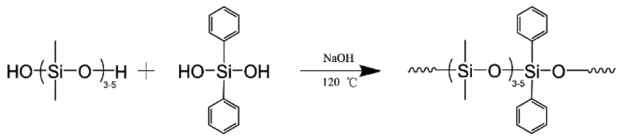


Fig. 1 Synthetic route of PPDMS.

Table 1 Fundamental formulation of phenyl silicone rubbers with different additives

| Samples | PPDMS (g) | Hydrophobic nano $SiO_2$ (g) | Microfiber glass wool (g) | $SiO_2$ (g) | $Al_2O_3$ (g) |
|---|---|---|---|---|---|
| PSR | 10.0 | 1.0 | — | — | — |
| PSR/MGW-2% | 10.0 | 1.0 | 0.2 | — | — |
| PSR/MGW-5% | 10.0 | 1.0 | 0.5 | — | — |
| PSR/MGW-10% | 10.0 | 1.0 | 1.0 | | — |
| PSR/$SiO_2$-5% | 10.0 | 1.0 | — | 0.5 | — |
| PSR/$Al_2O_3$-5% | 10.0 | 1.0 | — | — | 0.5 |

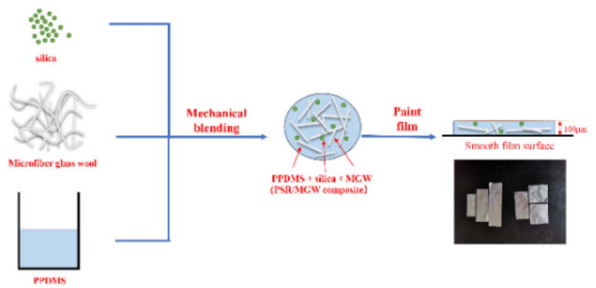


Fig. 2 Scheme of PSR/MGW composites.

C. The molecular weight range was determined to be between $1.26 \times 10^3$ and $3.85 \times 10^6$ g $mol^{-1}$.

Viscosity was measured using an NDJ-8S viscometer at 25 °C, in accordance with the GB/T21059-2007 standard.

Thermogravimetric analysis (TGA) was conducted in the temperature range of 25 to 800 °C using a thermal analyzer (STA 409 PC, NETZSCH, Germany) under a $N_2$ atmosphere with a flow rate of 20 mL $min^{-1}$. The sample size was set to 5–10 mg, and the heating rate was 10 K $min^{-1}$.

Dynamic mechanical analysis (DMA) was conducted in the temperature range of −120 °C to room temperature (+20 °C) using a dynamic mechanical analyzer (DMA 242) in the tensile mode. The testing frequency was set to 1 Hz, and the heating rate was 5 K $min^{-1}$.

**Scanning electron microscopy (SEM).** The cross-sectional morphology of the rubber samples was observed using a field-emission scanning electron microscope (Hitachi S-4800) at an accelerating voltage of 10.0–15.0 kV. The rubber samples were incubated in liquid nitrogen for 2 h and then quenched quickly to obtain the SEM samples.

**Optical property evaluation.** Infrared absorption performance of the material was evaluated using the transmission mode of an infrared spectrometer (Nicolet 6700, Thermo-Electron, USA). The original transmission spectrum recorded in the wavenumber range of 4000 to 400 $cm^{-1}$ was used to characterize the mid-infrared incident light absorption of the materials. The scanning frequency was 32 times per min. The solar transmission capability of the composite film was evaluated using a UV-vis spectrophotometer (UV765PC) and a spectrum analyzer (Spectrum Genius) to qualitatively characterize its solar absorptance. The wavelength range was 300 to 800 nm.

To evaluate the thermal conductivity of the material, its thermal diffusion coefficient was measured using a thermal conductivity meter (LFA467, NETZSCH, Germany) *via* the laser flash method under a $N_2$ atmosphere. The testing temperature range was 25–200 °C, with the testing points being 25, 50, 100, 150, and 200 °C; the heating rate was 10 K $min^{-1}$. Additionally, the specific heat of the material was measured through differential scanning calorimetry (DSC; DSC8500) using the standard sapphire method. DSC was performed under a nitrogen $N_2$

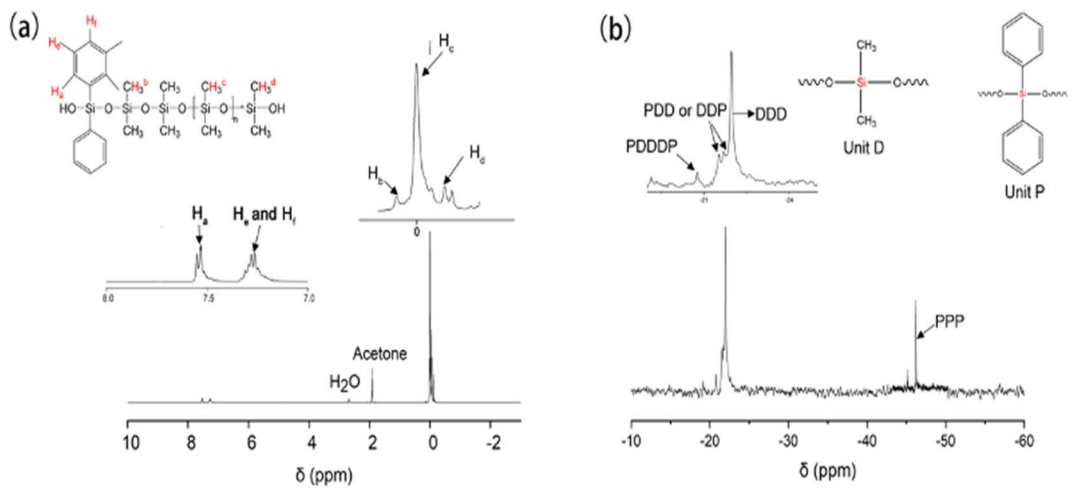


Fig. 3 $^{1}H$ NMR (a) and $^{29}Si$ NMR (b) spectra of PPDMS.

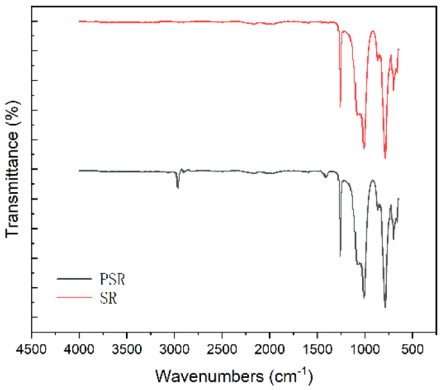


Fig. 4 Fourier transform infrared spectra of diphenyl silicone (PSR) and dimethyl silicone rubber (SR) samples.

atmosphere in the temperature range of 25–200 °C at a heating rate of 10 K $min^{-1}$.

The thermal conductivity coefficient was calculated as follows:

$$\lambda = c\rho\alpha \quad (1)$$

where $\lambda$ represents the thermal conductivity coefficient. $c$, $\rho$, and $\alpha$ represent the specific heat, density, and thermal diffusion coefficient of the material.

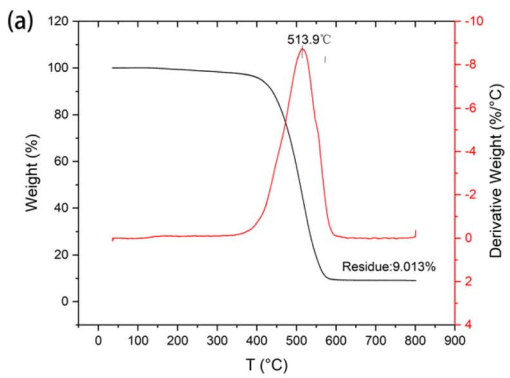


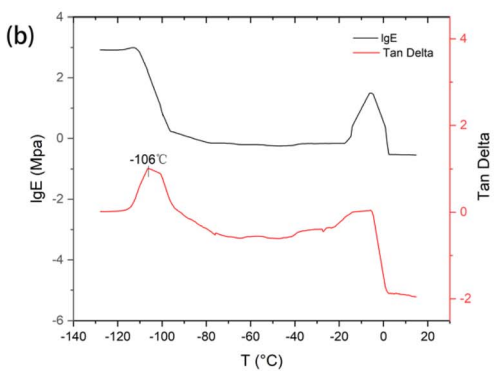


Fig. 5 TGA and DTG curves (a) and DMA curves (b) of PSR obtained under nitrogen.

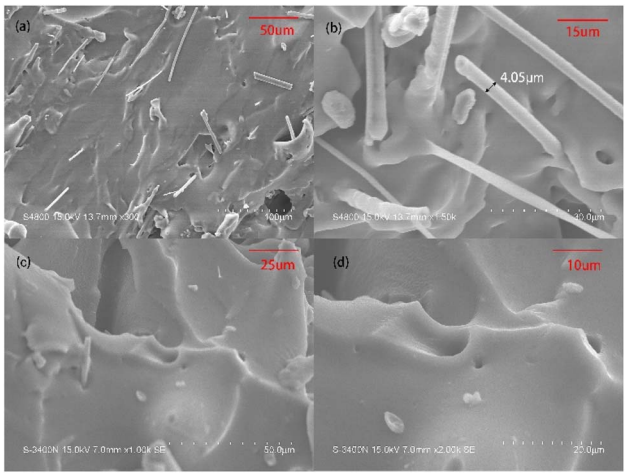


Fig. 6 SEM images of the quenched cross-sections of PSR/MGW-5 wt% (magnification: (a) 300× and (b) 1500×) and the PSR (magnification: (c) 1000× and (d) 2000×).

**Mechanical performance.** The linear expansion coefficient of the material was determined as follows: first, the test direction of the labeled specimen was identified, and the sample was placed in an aging oven. After being held at a constant temperature of 200 °C for 4 h, the sample was retrieved and its length, $L_0$ (unit: mm) was measured along the test direction. Once the test sample cooled to 20 °C, its length, $L_1$ was remeasured along the test direction. The measurement precision was 0.02 mm. The linear expansion coefficient of the sample was calculated as follows:

$$\text{Linear expansion coefficient } (\%) = \frac{L_0 - L_1}{L_0} \times 100\% \quad (2)$$

## Results and discussion

### Structural characterization of PPDMS and PSR

Fig. 3(a) presents the $^1$H NMR spectrum of PPDMS. The peak at 1.90 ppm corresponds to the protons of deuterated acetone and

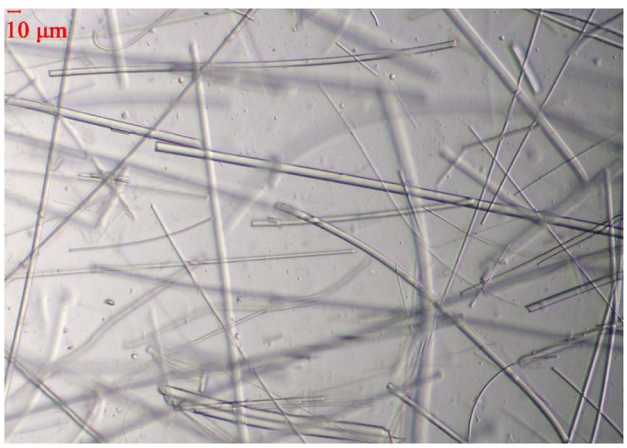


Fig. 7 Optical micrograph of the PSR/MGW-5 wt% (magnifying power: 100×).

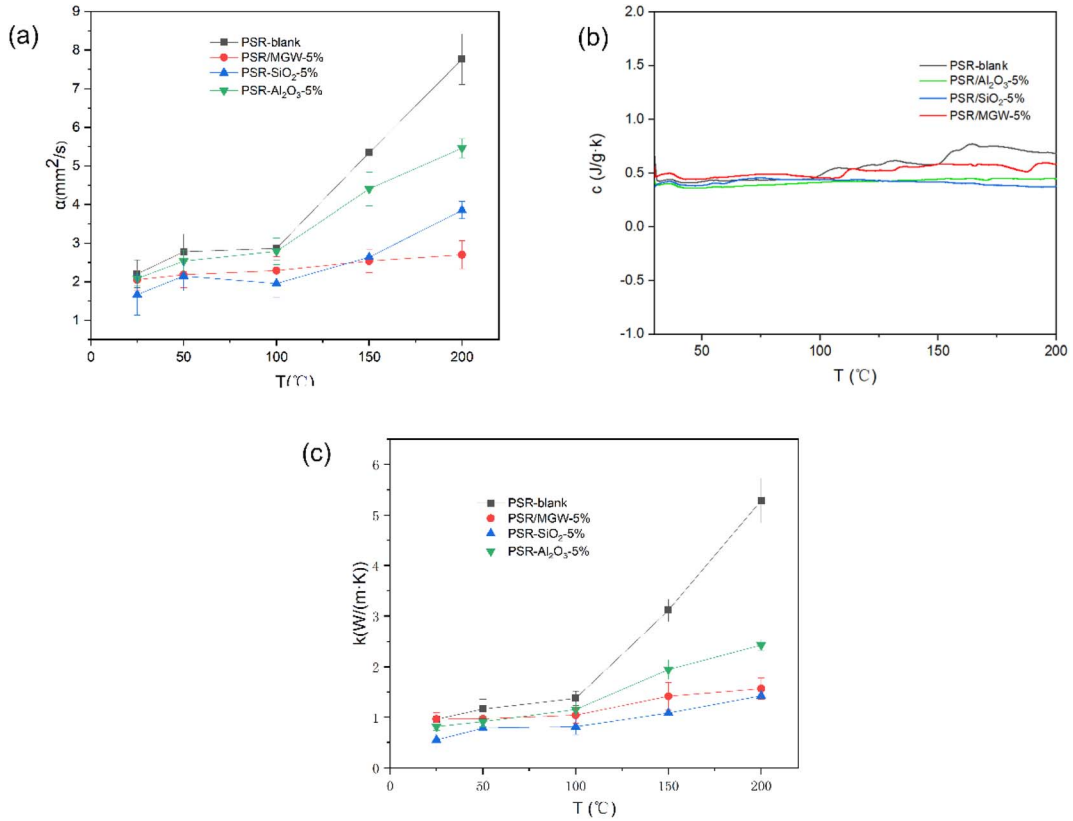


Fig. 8 Thermal diffusivity (a), specific heat (b), and thermal conductivity (c) of the PSR/inorganic filler hybrid film (thickness: 100 μm) with different inorganic fillers as a function of temperature in the 25–200 °C range.

that at 2.60 ppm corresponds to the water protons. The two doublet peaks between 7.20 and 7.55 ppm correspond to the protons of the diphenyl silicone structural unit, while the multiplet signals between −0.15 and +0.05 ppm correspond to the protons of the dimethyl silicone structural unit. These results indicate that the diphenyl silicone units were successfully copolymerized with the main chain of the dimethyl silicone rubber. The two doublet peaks appearing between 7.20 and 7.55 ppm correspond to the protons of PPDMS (the target product) rather than diphenylsilanediol (the reactant). The ratio of the integrated areas of the methyl signals to the phenyl ones is approximately 15 : 1. Through peak integration, the ratio of the dimethyl silicone structural unit to that of diphenyl silicone was calculated to be approximately 25 : 1, and the reaction efficiency of diphenylsilanediol was estimated to be approximately 60.0%.

$^{29}$Si NMR is currently the most effective method for characterizing the sequence structure of organosilicon polymers.[26,27] The $^{29}$Si NMR spectrum of PPDMS is presented in Fig. 3(b). Due to structural and sequential differences between the dimethyl silicone and diphenyl silicone structural units (referred to as the D and P units in Fig. 3(b)), multiple splitting peaks appeared in the $^{29}$Si NMR spectrum of PPDMS. The splitting peaks between −19.3 and −23.3 ppm are due to the presence of the D unit, while those with chemical shifts in the range of −46 to 48.5 ppm can be attributed to the P unit. Fig. 3 shows the structures formed by different arrangements of the D and P structural units and the corresponding signals in the $^{29}$Si NMR spectrum.

The infrared spectra of PSR and dimethyl silicone rubber (SR) are presented in Fig. 4. The dimethyl silicone rubber exhibited characteristic IR absorption peaks of Si–$CH_3$ at 1257 and 786 cm$^{-1}$, and Si–O–Si at 1071 and 1008 cm$^{-1}$. Compared to dimethyl silicone rubber, new characteristic absorption peaks of Si–$C_6H_5$ substituted with benzene appeared at 2962, 1412, and 698 cm$^{-1}$ in the sample. The presence of these characteristic absorption peaks indicates that the synthesized sample is a polymer containing a methylsiloxane segment and a benzene side group, which is consistent with the target product of diphenyl silicone rubber.

Table 2 Linear expansion coefficient of PSR/filler composites with different inorganic fillers after cooling from 200 to 20 °C

| Sample | $L_0$ (cm) | $L_1$ (cm) | Linear expansion coefficient (%) |
|---|---|---|---|
| PSR | 3.216 | 3.178 ± 0.002 | 1.18 ± 0.06 |
| PSR/MGW-2% | 3.332 | 3.298 ± 0.002 | 1.02 ± 0.06 |
| PSR/MGW-5% | 3.720 | 3.700 ± 0.002 | 0.53 ± 0.06 |
| PSR/MGW-10% | 3.010 | 2.996 ± 0.002 | 0.47 ± 0.06 |
| PSR/$SiO_2$-5% | 2.824 | 2.800 ± 0.002 | 0.85 ± 0.06 |
| PSR/$Al_2O_3$-5% | 3.112 | 3.090 ± 0.002 | 0.71 ± 0.06 |

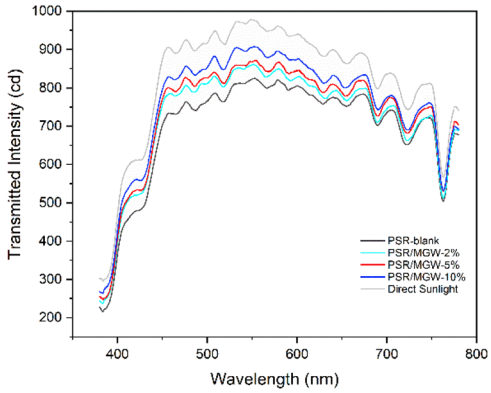


Fig. 9 Solar transmittance spectra of PSR/MGW hybrid films (thickness: 100 μm).

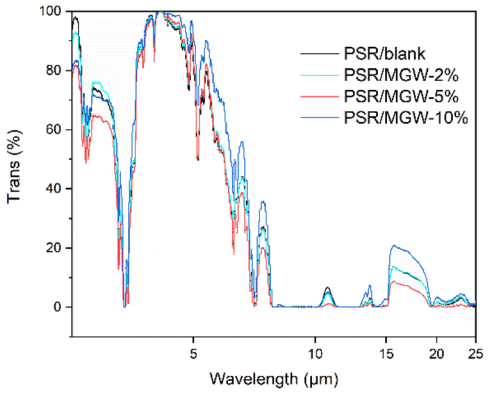


Fig. 10 Infrared transmission spectra of PSR/MGW hybrid films (thickness: 100 μm).

### Thermal stability and low-temperature performance of the PSR film

Polymeric materials used on spacecraft surfaces require good thermal stability and low-temperature performance to withstand the alternating high and low temperature environments. Fig. 4 shows the TGA and DMA curves of the PSR obtained in a nitrogen atmosphere. The TGA curve in Fig. 5(a) reveals that the $T_{onset}$ (the temperature corresponding to 5% weight loss) of the PSR is 410 °C. Further, only one peak appears in the derivative thermogravimetric (DTG) curve, and the maximum decomposition temperature, $T_{max}$ (the temperature corresponding to the maximum rate of weight loss), obtained from the DTG curve is 514 °C. This result indicates that PSR has good thermal stability and can meet the application requirements of spacecrafts. The introduction of diphenylsilane structural units improved the heat-resistance stability of the silicone rubber. This is because, in a $N_2$ atmosphere, the degradation mechanism of the silicone rubber is mainly cyclization and degradation caused by main chain rearrangement; that is, the Si–O bond in the main chain breaks to form low-molecular-weight cyclic siloxanes.[25,28,29] Diphenylsilane structural units have two effects on the PPDMS molecular chain: (i) they exert a large steric hindrance that can inhibit cyclization and degradation, and (ii) the electron-donating effect of the phenyl group weakens the positive charge of the adjacent silicon atoms, thereby increasing the stability of the rubber. In addition to improving the heat-resistance stability, the PSR also significantly enhances the UV-radiation resistance and other properties.[19–22,30,31]

The $T_g$ of dimethyl silicone rubbers is generally approximately −127 °C. However, in practical applications, owing to their regular molecular structure, symmetry, low cohesion energy, and easy movement of molecular chains, dimethyl silicone rubbers have a high tendency to crystallize at low temperatures, and the crystallization rate is fast. At −60 °C, the crystallinity reaches 60%. The elongation of dimethyl silicone rubbers at low temperature rapidly decreases over a very narrow temperature range, limiting their usage temperature range.[32]

The DMA results in Fig. 5(b) reveal that the damping peak temperature, which corresponds to the $T_g$ of the PSR sample with diphenylsilane units, is −106 °C, and there is no significant change in the storage or loss moduli in the temperature range of −80 to −40 °C. These results indicate that the PSR with diphenylsilane units has good cold resistance and can meet the application criteria of spacecrafts. Compared with the dimethyl silicone rubber, the PSR with phenyl groups has a higher $T_g$ and does not crystallize at temperatures exceeding its $T_g$. This result indicates that the introduction of diphenyl silicone structural units effectively suppresses the crystallization of the silicone rubber and improves its cold resistance. This is because diphenyl silicone rubber replaces the methyl groups at the terminal Si atoms with a large volume of rigid phenyl groups, thereby increasing steric hindrance. This reduces the regularity and mobility of the molecular chain structure of the PSR and increases its energy consumption, thus effectively reducing its crystallinity.[33]

### Dispersion of MGW in PSR

Fig. 6 displays the SEM images of the fracture surfaces of the PSR/MGW (5 wt%) and PSR samples at two different magnifications. As shown, the glass filler, MGW maintains its original morphology and is uniformly distributed with different orientations in the PSR matrix, forming the "skeletal structure" of the rubber. In addition, the interface between the MGW and rubber matrix is bound tightly, and the exposed surface of the MGW in the fracture section is smooth, indicating that there is a certain chemical bonding between the MGW and rubber matrix. It is possible that a small amount of the silanol groups on the surface of the MGW participates in the curing reaction of the silicone rubber.

Fig. 7 presents the dispersion of the MGW in the PSR matrix in the PSR/MGW sample (5 wt%). The results indicate that the glass microfibers maintain good structural integrity and are uniformly dispersed in the rubber matrix, suggesting that the grinding-based blending method does not disrupt the original structure of the MGW and can effectively disperse and bind it with the PSR matrix.

The addition of the glass microfibers can significantly improve the dimensional stability of the silicone rubber. Table 2

presents the linear expansion coefficients of the PSR films with different functional fillers after cooling from 200 to 20 °C.

### Thermal conductivity of the PSR samples

Fig. 8 presents the thermal diffusion coefficient, specific heat, and thermal conductivity curves of 100 μm thick phenyl-based silicone rubber films incorporated with different inorganic fillers in the temperature range of 25–200 °C. As shown, at room temperature, the addition of MGW, $SiO_2$, and $Al_2O_3$ did not have a significant effect on the thermal conductivity of the PSR film. However, at higher temperatures, the thermal diffusion coefficient of the PSR film with added MGW was significantly lower than that of the PSR film without the inorganic filler. When 5 wt% MGW was added, the thermal diffusion coefficient of the rubber composite film at 200 °C decreased from 7.765 to 2.703 mm $s^{-2}$. Additionally, among the composite films, the thermal conductivity of the PSR/MGW film exhibited the smallest change within the tested temperature range. This is because the MGW itself is a good thermal insulation material with low thermal conductivity.[34] Therefore, upon adding MGW, the thermal conductivity of the PSR film decreased, and its heating rate slowed at high temperatures, leading to good thermal insulation. At room temperature, the thermal conductivity of the rubber composite film was not affected, which is beneficial for timely heat dissipation on the surface of the satellite. Considering these two aspects, the prepared PSR/MGW film can effectively control heat exchange between the satellite surface and the frequently changing thermal environment surrounding it, thereby controlling the temperature changes of the satellite surface.

### Infrared absorption and solar transmittance properties of PSR films

In the thermal control process of spacecraft surfaces, solar absorptance $\alpha$ and infrared emittance $\varepsilon$ are two important parameters of thermal control coatings. Polymer film coatings with low solar absorptance and high infrared emittance (*i.e.*, low $\alpha/\varepsilon$ values) can effectively reduce the thermal equilibrium temperature of the substrate.[5] Such thin-film materials, together with vacuum-coated metal substrates, form second surface mirror-type thermal control coatings that have been widely applied on spacecrafts.[7]

Solar absorbance is the ratio of the absorbed visible radiation flux to incident radiation flux of the solar light. Fig. 9 shows the solar transmission spectra of 100 μm thick PSR/MGW films with different MGW contents. The integral area of the spectrum can qualitatively reflect the magnitude of solar absorbance. Based on the calculated integral area, under direct solar irradiation, the transmission intensity of the PSR control film is ~84.8% of the incident solar intensity, indicating that the PSR film itself has good visible-light transmittance. The transmission intensity of the PSR/MGW films was significantly higher than that of the PSR film, and the transmission intensity of the PSR/MGW composite film gradually increased with increasing MGW content. According to the calculated integral areas, the transmission intensities of the PSR/MGW-5 wt% and PSR/MGW-10 wt% films are approximately 89.9 and 92.7% of the incident solar intensity, respectively. This is because the MGW itself has good light-transmittance performance, and its refractive index is comparable to that of the PSR matrix. Thus, the loss caused by reflection and absorption when solar light passes through the PSR–MGW interface is smaller than that of the pristine PSR matrix. Therefore, the PSR/MGW composite film has a lower solar absorbance.

Infrared emittance refers to the ratio of the infrared spectral emissive power of the substrate surface to that of a black body at the same temperature and wavelength. It is a commonly used parameter to characterize the thermal radiation ability of materials in the infrared region. Fig. 10 presents the infrared transmission spectra in the wavelength range of 2.5 to 25 μm for 100 μm thick PSR/MGW films with different MGW contents. The integrated area above each spectrum reflects the strength of the infrared absorption capability of the material. The results suggest that PSR itself has good infrared absorption characteristics; it exhibits almost 100% absorption of the infrared light in the 7.5–15 and 20–25 μm ranges. This is because the Si–O–Si structure in the PSR strongly absorbs the 10 μm IR wavelength, and the methyl groups in $Si–CH_3$ exhibit strong infrared absorption at 15 μm. The hydrophobic nano-$SiO_2$ added as a reinforcing material has strong infrared absorption in the 20–25 μm range. After the addition of MGW, no significant change in the overall infrared absorption of the PSR film was observed; however, the infrared absorption in local regions was enhanced. According to Kirchhoff's law, at the same temperature, the infrared absorption of a material is proportional to its infrared radiation. Therefore, PSR films have a relatively high infrared radiation rate.

From these two perspectives, the prepared PSR/MGW film has a low $\alpha/\varepsilon$ value and thus has good ability to control the equilibrium temperature. This feature renders it suitable as a thermal control coating of spacecrafts.

## Conclusion

(1) PSR, a rubber with biphenylsiloxane structural units was prepared by a co-condensation reaction. $^1H$ and $^{29}Si$ NMR spectroscopic studies revealed that PSR contained 3.8 mol% of biphenylsiloxane structural units, which were uniformly distributed in polydimethylsiloxane chains. DMA and TGA revealed that the prepared silicone rubber with phenyl groups has good thermal stability and low-temperature resistance, and has a glass transition temperature of −106 °C and a decomposition temperature exceeding 410 °C.

(2) The glass filler, MGW was uniformly dispersed in the PSR matrix using a grinding-based blending method to obtain a dimensionally stable PSR/MGW composite film. The so-obtained films exhibited good visible-light transmission and low $\alpha/\varepsilon$ values, allowing effective control of the surface temperature of the substrate. Additionally, the thermal conductivity of the film did not change significantly within the operating temperature range (25–200 °C). Therefore, the organic/inorganic hybrid composite film is suitable as a surface

thin-film material for secondary mirror thermal control coatings and has application potential in the aerospace industry.

## Author contributions

Lin Li: conceptualization, investigation, data curation, writing – original draft preparation. Xin Fu: formal analysis. Xiang Xu: conceptualization, methodology, formal analysis. Dafu Wei: validation. Yong Guan: writing – review & editing.

## Conflicts of interest

There are no conflicts to declare.

## Acknowledgements

We gratefully acknowledge the financial support from the National Natural Science Foundation of China (No. 21805086), Shanghai Leading Academic Discipline Project (B502), and the Shanghai Key Laboratory Project (Grant No. ZD20170203).

## Notes and references

1 S. Wijiewardane and D. Y. Goswami, A review on surface control of thermal radiation by paints and coatings for new energy applications, *Renewable Sustainable Energy Rev.*, 2012, **16**, 1863–1873.

2 D. A. Jaworske, Correlation of predicted and observed optical properties of multiplayer thermal control coatings, *Thin Solid Films*, 1998, **332**, 30–33.

3 J. A. Dever, E. J. Bruckner and E. Rodriguez, Synergistic effects of ultraviolet radiation, thermal cycling and atomic oxygen on altered and coated Kapton surfaces, *American Institute of Aeronautics and Astronautics 30th Aerospace Sciences Meeting and Exhibit*, Reno, NV, USA, 1992, DOI: 10.2514/6.1992-794.

4 K. Shimazaki, A. Ohnishi and Y. Nagasaka, Development of spectral selective multilayer film for a variable emittance device and its radiation properties measurements, *Int. J. Thermophys.*, 2003, **24**, 757–769.

5 T. Ozawa, Temperature control modes in thermal analysis, *J. Therm. Anal. Calorim.*, 2001, **64**, 109–126.

6 X. Li, Z. P. Yao, X. J. Li, H. Xu, Q. X. Xia, C. J. Chen and Z. H. Jiang, Application of micro-arc oxidation technology in thermal control coating, *Surf. Technol.*, 2019, **48**, 24–36.

7 Q. Mu, Y. Liu, D. Peng, J. Li, L. Wang and M. Zhang, Study on Properties of Methylphenyl Silicone Materials for LED Packaging, *Silicone Mater.*, 2013, **27**, 10–14.

8 N. Kayhan, R. S. Razavi and S. Choopani, Evaluation of two new white silicone thermal control paints under atomic oxygen, *Prog. Org. Coat.*, 2012, **74**, 603–607.

9 D. Li, W. Yang and X. Liu, Radiative properties of second surface mirror type thermal control coatings, *Spacecr. Environ. Eng.*, 2013, **30**, 196–199.

10 M. Holynska, A. Tighe and C. Semprimoschnig, Coatings and Thin Films for Spacecraft Thermo-Optical and Related Functional Applications, *Adv. Mater. Interfaces*, 2018, 1701644, DOI: 10.1002/admi.201701644.

11 S. Diao, S. Zhang, Z. Yang, S. Feng, C. Zhang, Z. Wang and G. Wang, Effect of Tetraphenylphenyl-Modified Fumed Silica on Silicone Rubber Radiation Resistance, *J. Appl. Polym. Sci.*, 2011, **120**, 2440–2447.

12 L. Zhang, C. Yan, Q. Qu, G. Shun and J. Tong, Performance of organic silicone thermal control coatings for space craft, *Corros. Sci. Prot. Technol.*, 2003, **1**, 21–23.

13 J. Jiang, J. Wang, Z. Wang, J. Chen, A. Cao, R. Zhao and X. Hu, Experimental research on atomic oxygen effect of thermal control coatings, *Spacecr. Eng.*, 2004, **2**, 32–35.

14 X. Wang, X. Zhao and Z. Shen, The effects of atomic oxygen on epoxy resin containing organosilicon, *J. Astronaut.*, 2006, **27**, 1113–1117.

15 C. L. Zhu, Y. Z. Wei, J. Zhang, P. F. Geng and Z. J. Lu, Preparation of polysiloxane oligomers bearing benzoxazine side groups and tunable properties of their thermosets, *J. Appl. Polym. Sci.*, 2014, **131**, 40960.

16 P. Norman, T. E. Schwartzentruber, H. Leverentz, S. Luo, R. Meana-Pañeda, Y. Paukku and D. G. Truhlar, The structure of silica surfaces exposed to atomic oxygen, *J. Phys. Chem. C*, 2013, **117**, 9311–9321.

17 H. Wang, M. J. Vanessa, M. K. Timothy, D. Dai, B. Wu, Y. Yang and C. Li, Study on the resistance of thermal control coating of phenyl silicone rubber to hyperthermal atomic oxygen attack, *J. Astronaut.*, 2017, **38**, 662–668.

18 D. Shen, K. Jin, Z. Yang, H. Lu, S. Feng and C. Zhang, The effect of phenyl modified fumed silica on radiation resistance of silicone rubber, *Mater. Chem. Phys.*, 2011, **4**, 31–34.

19 Z. Jiang, J. Zhang and S. Feng, Effects of polymethylvinylsilicone oil with side tetraphenylphenyl groups on the radiation resistance of addition-type silicone rubber, *J. Appl. Polym. Sci.*, 2007, **104**, 4144–4148.

20 Z. Jiang, J. Zhang and S. Feng, Effects of polymethylvinylsilicone oil with condensed aromatics on the radiation resistance of addition-type silicone rubber, *J. Appl. Polym. Sci.*, 2006, **12**, 1937–1942.

21 Y. Wang, R. Cao, M. Wang, X. Liu, X. Zhao, Y. Lu, A. Feng and L. Zhang, Design and synthesis of phenyl silicone rubber with functional epoxy groups through anionic copolymerization and subsequent epoxidation, *Polymer*, 2019, 122077.

22 Y. Li, G. Liu, K. Cao, C. Peng, B. Zhou, Y. Pan and Z. Chen, Research on POSS-modified thermal control white coating for satellite, *Paint Coat. Ind.*, 2017, **47**, 6–12.

23 A. Vlad, M. Cazacu, M. Marcu and C. Racles, Synthesis of poly(dimethyldiphenylsiloxane) alpha, omega-diol copolymers by acid-catalyzed polycondensation, *Rev. Roum. Chim.*, 2001, **46**, 919–924.

24 X. Xu, Z. Xu, P. Chen, X. Zhou, A. Zheng and Y. Guan, Preparation of Fluorosilicone Random Copolymers with Properties Superior to Those of Fluorosilicone/Silicone Polymer Blends, *J. Inorg. Organomet. Polym.*, 2015, **25**, 1267–1276.

25 Y. You, A. Zheng, D. Wei, X. Xu, Y. Guan and J. Chen, Improving the thermal stability of poly [methyl(trifluoropropyl)siloxane] by introducing diphenylsiloxane units, *RSC Adv.*, 2023, **13**, 11424–11431.
26 I. R. Hebert and A. D. H. Clague, Detailed structural analysis of polysiloxane antifoam agents using carbon-13 and silicone-29 NMR spectroscopy, *Macromolecules*, 1989, **22**, 3267–3275.
27 J. Shi, N. Zhao, S. Xia, S. Liu and Z. Li, Phosphazene superbase catalyzed ring-opening polymerization of cyclotetrasiloxane toward copolysiloxanes with high diphenyl siloxane content, *Polym. Chem.*, 2019, **10**, 2126–2133.
28 Y. R. Liu, Y. D. Huang and L. Liu, Thermal stability of POSS/methylsilicone nanocomposites, *Compos. Sci. Technol.*, 2007, **67**, 2864–2876.
29 N. Grassie, K. F. Francey and I. G. Macfrlane, The thermal degradation of polysiloxanes - part 4: poly(dimethyl/diphenyl siloxane), *Polym. Degrad. Stab.*, 1980, **2**, 67–83.
30 H. Wei, Y. Fu, C. Wang, Y. Xu and Z. Bian, A study on radiation resistance of siloxane foam containing phenyl, *Radiat. Phys. Chem.*, 2002, **64**, 229–233.
31 R. S. Maxwell, R. Cohenour, W. Sung, D. Solyom and M. Patel, The effects of g-radiation on the thermal, mechanical, and segmental dynamics of a silica filled, room temperature vulcanized polysiloxane rubber, *Polym. Degrad. Stab.*, 2003, **80**, 443–450.
32 J. Zhao, P. Chen, Y. Lin, W. Chen, A. Lu, L. Meng, D. Wang and L. Li, Stretch-induced intermediate structures and crystallization of poly(dimethylsiloxane): the effect of filler content, *Macromolecules*, 2020, **53**, 719–730.
33 Y. Huang, Q. Mu and Z. Su, High and low temperature of phenyl silicone rubber, *IOP Conf. Ser.: Mater. Sci. Eng.*, 2021, **1048**, 012001.
34 X. Yan, X. Huang, G. Sun and Y. M. Xie, Two-scale optimal design of structures with thermal insulation materials, *Compos. Struct.*, 2015, **120**, 358–365.